

Efficient Determination of Relative Entropy Using Combined Temperature and Hamiltonian Replica-Exchange Molecular Dynamics

Sunhwan Jo,[†] Christophe Chipot,^{‡,§,||} and Benoît Roux^{*,#,⊥}

[†]Argonne Leadership Computing Facility, Argonne National Laboratory, 9700 South Cass Avenue, Building 240, Lemont, 60439 Illinois, United States

[‡]Laboratoire International Associé Centre National de la Recherche Scientifique and University of Illinois at Urbana–Champaign, UMR 7565, Université de Lorraine, BP 70239, 54506 Vandœuvre-lès-Nancy, France

[§]Department of Physics, University of Illinois at Urbana–Champaign, 1110 West Green Street, Urbana, Illinois 61801, United States

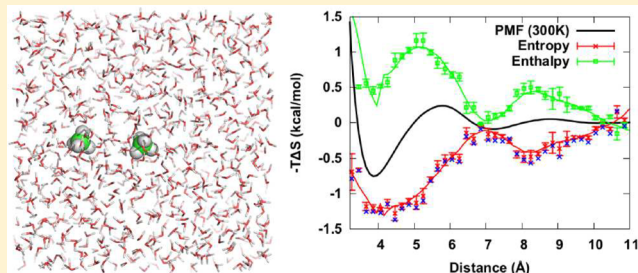
[#]Beckman Institute for Advanced Research and Technology, University of Illinois at Urbana–Champaign, 405 North Mathews, Urbana, Illinois 61801, United States

[⊥]Department of Biochemistry and Molecular Biology, Gordon Center for Integrative Science, University of Chicago, Chicago, Illinois 60637, United States

^{*}Center for Nanoscale Materials, Argonne National Laboratory, 9700 South Cass Avenue, Building 440, Argonne, Illinois 60439, United States

Supporting Information

ABSTRACT: The performance and accuracy of different simulation schemes for estimating the entropy inferred from free energy calculations are tested. The results obtained from replica-exchange molecular dynamics (REMD) simulations based on a simplified toy model are compared to exact numerically derived ones to assess accuracy and convergence. It is observed that the error in entropy estimation decreases by at least an order of magnitude and the quantities of interest converge much faster when the simulations are coupled via a temperature REMD algorithm and the trajectories from different temperatures are combined. Simulations with the infinite-swapping method and its variants show some improvement over the traditional nearest-neighbor REMD algorithms, but they are more computationally expensive. To test the methodologies further, the free energy profile for the reversible association of two methane molecules in explicit water was calculated and decomposed into its entropic and enthalpic contributions. Finally, a strategy based on umbrella sampling computations carried out via simultaneous temperature and Hamiltonian REMD simulations is shown to yield the most accurate entropy estimation. The entropy profile between the two methane molecules displays the characteristic signature of a hydrophobic interaction.



INTRODUCTION

Free energy is often the most important quantity in order to understand the thermodynamic forces governing complex biological phenomena. Given an atomic model, computational methods can be brought to bear on the determination of the free energy variations along a microscopic process. For example, the potential of mean force (PMF) along a model reaction coordinate can be calculated using umbrella sampling (US) simulations. Constructing free energy profiles under different thermodynamic conditions, e.g., protonation states, charges, or temperatures, provides valuable insight into chemical and biological processes. Toward a complete characterization of a molecular process, it is sometimes desirable to determine additional thermodynamic variables, such as enthalpy, entropy, and heat capacity. In particular, entropy is known to play an important role in many chemical

and biological processes, such as hydrophobic interaction,^{1–3} allostery,^{4,5} and molecular recognition.^{6–8} Thus, having the ability to accurately determine entropy using computer simulations is expected to greatly help theoretical studies of complex biomolecular processes.

Using conventional MD simulation methods, accurate estimation of entropy and enthalpy can become extremely challenging due to the large fluctuations in the energy and entropy, which are proportional to the number of degrees of freedom.^{9,10} A typical biological system is composed of tens of thousands of atoms including solvent, rendering a direct estimation of entropy via conventional simulation nearly impossible. Alternatively, estimating the entropy via a finite

Received: November 20, 2014

difference (FD) of the free energy with respect to temperature, $\Delta S = -\partial \Delta F / \partial T \approx -[\Delta F(T + \Delta T) - \Delta F(T - \Delta T)]/2\Delta T$, offers an attractive and viable computational route that has been widely used.^{11–13} In the FD approach, the entropy is commonly estimated by carrying out separate simulations performed at different temperatures. The performance of the FD approach has been compared to that of other available methods, such as thermodynamic integration or free energy perturbation approaches, but the FD approach appears to be performing comparable to or better than the other aforementioned alternatives.^{11,14}

Although the FD approach performs generally well, a significant amount of sampling and large temperature gaps between simulation systems are required to ensure statistically meaningful estimation of entropy due to large fluctuations in biologically relevant simulation systems. To avoid large statistical error from the fluctuations in the free energy, large temperature increments ($\Delta T > 20$ K) between simulations are typically used, under the assumption of constant heat capacity.^{11,15} While this assumption is generally good,¹⁶ the practitioner must be aware that the FD approximation breaks down if the temperature gap is too large and the entropy estimates become inaccurate.

The efficiency of entropy estimation can be enhanced by advanced sampling and analysis techniques. Sampling of phase space at the temperature of interest can be enhanced by sampling nearby thermodynamic states using temperature replica-exchange molecular dynamics (*T*-REMD).¹⁷ The data collected by sampling different temperatures can be combined by means of the temperature-weighted histogram analysis method (*T*-WHAM), which produces reliable ensemble averages at the target temperature.^{14,18,19} Rick¹⁴ showed that by combining *T*-REMD and *T*-WHAM the accuracy of entropy estimation can be significantly enhanced in the free energy calculation. Similarly, increased efficiency and accuracy in the prediction of simple polypeptide structures has been observed when Hamiltonian and *T*-REMD approaches are combined.^{20,21}

Here, we combine an umbrella sampling (US) method with the FD approach to decompose the entropy and enthalpy contributions along a reaction's coordinates. To enhance the convergence of the PMFs and estimated entropy, we will adopt either or both Hamiltonian and *T*-REMD methods. The performance of the different simulation and analysis methodologies will be assessed using a toy model system, whose PMFs and entropy profiles can be numerically obtained. Finally, we apply the methodology to the association of two methane molecules in liquid water and dissect the entropic and enthalpic contributions.

METHODS

Toy Simulation System. To illustrate the efficiency of the various entropy estimation methods, we have used a simplified toy simulation system composed of a single particle moving within the (x,y) plane with the following energy function

$$U(x,y) = -80 \left(\frac{1}{\sqrt{x^2 + (y - 5)^2 + 9}} + \frac{1}{\sqrt{(x - 10)^2 + (y - 10)^2 + 16}} + \frac{1}{\sqrt{(x - 10)^2 + (y - 5)^2 + 38}} + \frac{1}{\sqrt{(x - 10)^2 + y^2 + 16}} \right) \quad (1)$$

The energy function along the x axis and the energy surface along the (x,y) plane are shown in Figure 1. A flat bottom harmonic potential is applied so that the particle is free to move within $(-10 < x < 20)$ and $(-10 < y < 20)$ while its degree of freedom along the z direction is restricted using a harmonic restraint potential with a large force constant. This energy function can be integrated numerically using the Boltzmann factor, $\int_y \exp[-U(x,y)/k_B T]$, to yield a one-dimensional free

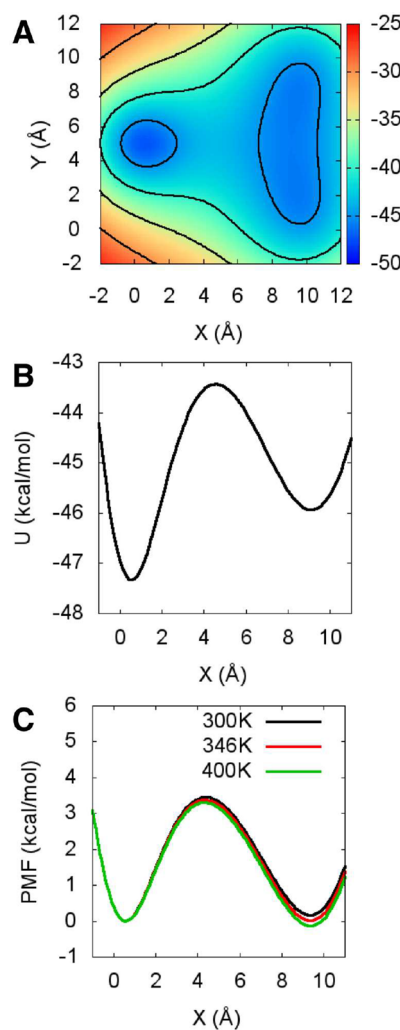


Figure 1. Energy function of the toy model. (A) 2D energy of the toy model in the (x,y) plane. (B) Potential energy of the system as the particle moves along the x axis, with $Y = 0$. (C) 1D PMF along the x axis obtained by numerical integration of the Boltzmann factor at three different temperatures.

energy surface along the x axis. The PMF can be evaluated at different temperatures (Figure 1C), and the entropy obtained by numerical integration can be used to compare the entropy profiles derived from alternative simulation and analysis schemes.

Calculation of PMF and Entropy. The US/(\mathcal{H}, T)-REMD method exchanges the window parameters, using a neighbor-exchange scheme with alternating neighbor lists either along the intermolecular distance bias or along the temperature. In the neighbor-exchange scheme, swapping the window conditions for neighboring replicas i and j is attempted at regular intervals. In the isothermal, isobaric ensemble, the swap is accepted according to the acceptance criterion

$$\begin{aligned} P_{\text{accept}}(i \leftrightarrow j) \\ = \min[1, \exp[-(\beta_j - \beta_i)(U_0(R_j) + pV_j - U_0(R_i) - pV_i) \\ - \beta_j(w_j(R_j) - w_i(R_i)) - \beta_i(w_i(R_i) - w_j(R_j))] \quad (2) \end{aligned}$$

where U_0 represents the unperturbed potential energy and p represents the pressure of the simulation system. R_i , V_i , w_i , and β_i are the coordinates, volume, biasing potential, and the inverse temperature $1/k_B T$ of replica i , respectively. The umbrella sampling replica-exchange script shipped with the original NAMD distribution was modified to perform bias and temperature replica-exchange simulations. The toy model together with the bias and the modified temperature exchange scripts will be made available via Github source repository.

The simulation trajectories have been analyzed using WHAM^{22,23} to produce the PMFs. Here, we used both the conventional WHAM²⁴ for umbrella sampling and T-WHAM approaches.^{14,18,19} In T-WHAM, the unbiased probability ρ_0 along the reaction coordinates η at target inverse temperature β_0 is described as

$$\begin{aligned} \rho_0(\eta, U | \beta_0) \\ = \sum_{i=1}^N \frac{n_i \exp[-\beta_0 U]}{\sum_{j=1}^N n_j \exp[f_j - \beta_j W_j(\eta) - \beta_j U]} \rho_i^{(b)}(\eta, U | \beta_i) \quad (3) \end{aligned}$$

where N is the total number of replicas, n_i is the number of data points collected from replica i , and U is the potential energy of the system. $\rho_i^{(b)}$ is the biased probability distribution obtained from the umbrella sampling simulations. In the isothermal-isobaric ensemble, the enthalpy, $H = U + pV$, is used instead.¹⁴ The dimensionless free energy, f_i , is computed as

$$\begin{aligned} e^{-f_i} \\ = \int dU \int d\eta \exp[-\beta_i W_i(\eta) - (\beta_i - \beta_0)U] \rho_0(\eta, U | \beta_0) \\ = \sum_{i=1}^N \sum_{m=1}^{n_i} \frac{n_i \exp[-\beta_i W_i(\eta) - \beta_i U]}{\sum_{j=1}^N n_j \exp[f_j - \beta_j W_j(\eta) - \beta_j U]} \delta(\eta - \eta_{i,m}) \delta(U - U_{i,m}) \\ = \sum_{i=1}^N \sum_{m=1}^{n_i} \frac{\exp[-\beta_i W_i(\eta_{i,m}) - \beta_i U_{i,m}]}{\sum_{j=1}^N n_j \exp[f_j - \beta_j W_j(\eta_{i,m}) - \beta_j U_{i,m}]} \quad (4) \end{aligned}$$

The resulting unbiased probability $\rho_0(\eta, U | \beta_0)$ can be summed over discretized energy bins to produce the probability along the reaction coordinates η , which can then be used to calculate the corresponding PMF.

$$W(\eta) = -\beta_0^{-1} \log \rho_0(\eta) = -\beta_0^{-1} \log \sum_l \rho_0(\eta, U_l | \beta_0) \quad (5)$$

The entropy along the reaction coordinates can be calculated by taking the temperature derivative of $W(\eta)$ using the FD approach, $\Delta S(\eta) = -[W(\eta, T + \Delta T) - W(\eta, T - \Delta T)]/2\Delta T$, and the enthalpy contribution is simply given by $\Delta H(\eta) = W(\eta) - T\Delta S(\eta)$. Alternatively, the entropy can be estimated using free energy perturbation approach¹¹

$$\Delta S(\eta) = -\left(\frac{\partial W(\eta)}{\partial T}\right) = \frac{\langle U(\eta) \rangle - \langle U \rangle - W(\eta)}{T} \quad (6)$$

where $\langle U(\eta) \rangle$ represents the average energy along the reaction coordinates, which can be easily calculated using the weights from the T-WHAM algorithm

$$\langle U(\eta, \beta) \rangle = \frac{\sum_l U_l \rho_0(\eta, U_l | \beta)}{\sum_l \rho_0(\eta, U_l | \beta)} \quad (7)$$

In this work, entropies are estimated using the FD approach unless stated otherwise.

Using the FD approach, multiple entropy estimations are possible depending on the temperature pairs utilized when more than two simulations were performed. For example, if three simulations were performed at three different temperatures (e.g., $T - \Delta T$, T , and $T + \Delta T$), then three estimates of the entropy can be inferred from finite differences using $(T - \Delta T$ and T), $(T - \Delta T$ and $T + \Delta T$), and $(T$ and $T + \Delta T$). Because entropy is constant within a range of temperatures, we have used standard deviations of these multiple entropy estimates to determine the uncertainty associated with the entropy estimation.

Partial Infinite Swapping. The quality of the entropy estimation depends on how well phase space is sampled. Thus, we have adopted REMD to enhance the efficiency of sampling. It has been suggested that the efficiency of REMD can be further increased as the replica-exchange frequency increases,^{25,26} and Dupuis et al. mathematically showed that the efficiency of the replica exchange, indeed, increased as replicas are exchanged more frequently and maximized at the limit of infinite swapping.²⁷ On the basis of this idea, Plattner et al. proposed infinite swapping (INS) and partial infinite swapping (PINS) algorithms and showed that the sampling efficiency can be better than that of T-REMD.^{28,29}

The INS method allows rapid mixing of replicas in generalized ensemble simulations by rearranging replica conditions based on the probability of all possible arrangements of replica conditions, given the configuration of replicas instead of attempting to exchange only neighbors as in typical replica-exchange schemes. For example, for a system composed of N replicas having a set of configurations \mathbf{X} , the permutation probability $p_k(\mathbf{X})$ of having a set of replica conditions arranged in a particular order, k , is given by

$$\rho_k(\mathbf{X}) = \frac{p_k(\mathbf{X})}{\sum_l^{N!} p_l(\mathbf{X})} \quad (8)$$

with $p_k(\mathbf{X})$ is given by

$$p_k(\mathbf{X}) = \exp[-\beta_1 U(x_{k,1}) - \beta_2 U(x_{k,2}) \dots - \beta_N U(x_{k,N})] \quad (9)$$

where $x_{k,n}$ represents the configuration of replica n according to the arrangement of replica conditions, k . For each cycle,

permutation probabilities are calculated, the next replica arrangement is randomly selected using the permutation probabilities as weights, and the new replica conditions are assigned to each replica. The INS method accelerates the travel of replicas in the replica condition space. It, however, requires evaluation of all possible outcomes of exchanges, which is $N!$ for a system having N replicas. The PINS method defines smaller, nonoverlapping blocks, where permutational probabilities are fully computed within the block, thus reducing the computing cost substantially. The configuration of blocks are rearranged at regular intervals to ensure the complete traversal of the replica.

INS can be seen as an independent sampling algorithm used in a Gibbs sampler,³⁰ and a similar, albeit simpler, scheme has been applied in earlier literatures.^{31,32} Although INS is expected to accelerate the mixing of replicas, there is a non-zero probability that replicas remain with the same arrangement. Because the next configurations are simply selected based on the permutation probability, if the permutation probabilities of staying with the same configuration is large, then the replicas will stay in the same arrangement and no gain in sampling efficiency will be observed.

Liu³³ has proved that the efficiency of the independent sampling can be further enhanced by always attempting to exchange configurations different from the current configuration and using Metropolis–Hastings criterion for acceptance of such exchange. Later, Chodera and Shirts³⁰ also empirically showed an improved efficiency for a simple system. We have implemented a Metropolized version of PINS (M-PINS) and explored the efficiency compared to that of REMD and PINS. In M-PINS, the next configuration is randomly picked based on the weight $\alpha(i \rightarrow j)$, calculated by

$$\alpha(i \rightarrow j) = \begin{cases} \frac{\rho_j}{1 - \rho_i} & (\text{for } i \neq j) \\ 0 & (\text{for } i = j) \end{cases} \quad (10)$$

where i and j represent the current and proposed configurations, respectively. Once the new configuration is selected, the proposed configuration is either accepted or rejected with an acceptance probability

$$P_{\text{accept}}(i \rightarrow j) = \min \left\{ 1, \frac{1 - \rho_i}{1 - \rho_j} \right\} \quad (11)$$

The acceptance criterion is chosen to satisfy detailed balance. When there are only two replicas in a block, M-PINS reduces to the regular replica-exchange algorithm. We have implemented PINS for umbrella sampling and temperature replica-exchange simulations within the popular simulation package NAMD, and the source code will be made available in a Github repository.

Multiple-Walker Adaptive Biasing Force. Among the variety of importance-sampling schemes available to the practitioner, the adaptive biasing force (ABF) method^{34,35} has proven to be an effective route toward variance reduction. In the course of the simulation, the algorithm estimates locally the required biasing force to yield a Hamiltonian devoid of an average force acting along the transition coordinate. It follows that all values of the latter are sampled with roughly the same probability, which, in turn, greatly improves the accuracy of the computed free energy differences.^{15,34,35} In stark contrast with

probability-based methods, such as umbrella sampling, the present approach uses a purely local estimate of the free energy derivative so that the time-dependent biasing force is updated continuously.

Performance of the adaptive biasing algorithm is evidently largely subservient to time scale separation and how decoupled the model reaction coordinate is from other, slow degrees of freedom.^{36,37} In concrete molecular systems, notably those of biological relevance, sampling is often thwarted by hidden, virtually insurmountable free energy barriers in the direction orthogonal to the transition coordinate. This common shortcoming can be understood in terms of an oversimplification of the representation of the reaction coordinate, often by means of a one-dimensional collective variable. To enhance sampling, one possible communication strategy, coined shared or multiple-walker ABF, consists of collecting force samples from each walker in a shared buffer as the simulations simultaneously proceed.^{38,39} The idea of a shared buffer is purely conceptual, as, in practice, force samples are synchronized periodically among the different walkers. The performance of the algorithm has proven to be spectacular in the case of markedly rugged free energy landscapes and the use of a model reaction coordinate for which a single-walker simulation is unable to recover the global minimum in a heap of highly degenerated conformational states.

Computational Detail. All MD simulations were carried out using NAMD simulation package.⁴⁰ For the toy simulation system, a Langevin thermostat was used with a friction coefficient of 5 ps^{-1} and a time step of 1 fs. In US simulation, a total of 28 windows ranging from $x = -2$ to 12 \AA were used and harmonic restraining potentials evenly separated by 0.5 \AA along the x axis were applied with a force constant of 5 kcal/mol· \AA^2 . For US/(\mathcal{H}, T)-REMD simulation, three temperature windows were used, ranging from 300 to 400 K, in conjunction with US windows, which yielded a total of 84 windows.

For the methane dimer simulations, the topology and parameters of methane⁴¹ and the modified TIP3P water model of the CHARMM force field^{42,43} were employed. The two methane molecules were solvated in a $30 \times 30 \times 30 \text{ \AA}^3$ pre-equilibrated water box. The solvated system was equilibrated for 500 ps in the isobaric–isothermal ensemble. A time step of 2 fs with the SHAKE algorithm was adopted.⁴⁴ van der Waals interactions were smoothly truncated at $10\text{--}12 \text{ \AA}$ by a force-switching function,⁴⁵ and the long-range electrostatic interactions were calculated using the particle-mesh Ewald method.⁴⁶ The temperature control was achieved by Langevin thermostat with a friction coefficient of 1 ps^{-1} . The constant pressure was maintained at 1.01325 bar by using Nosé–Hoover Langevin piston^{47,48} with a piston period of 50 fs and a piston decay of 25 fs.

For the US/(\mathcal{H}, T)-REMD simulations of methane dimer, a total of 75 windows (15 intermolecular distance windows and 5 temperature windows) were used. The intermolecular distance windows ranging from $r = 3.5$ to 10.5 \AA , and harmonic restraining potentials evenly separated by 0.5 \AA along the x axis were applied with a force constant of 5 kcal/mol· \AA^2 for each window. The temperature windows span from 295 to 305 K, and the exponential temperature spacing scheme was used, which resulted in temperature windows of 295, 297.46, 299.96, 302.47, and 305 K. The time interval of attempted exchange was set to 100 steps, and the position of the particles was recorded for postanalysis at the same interval.

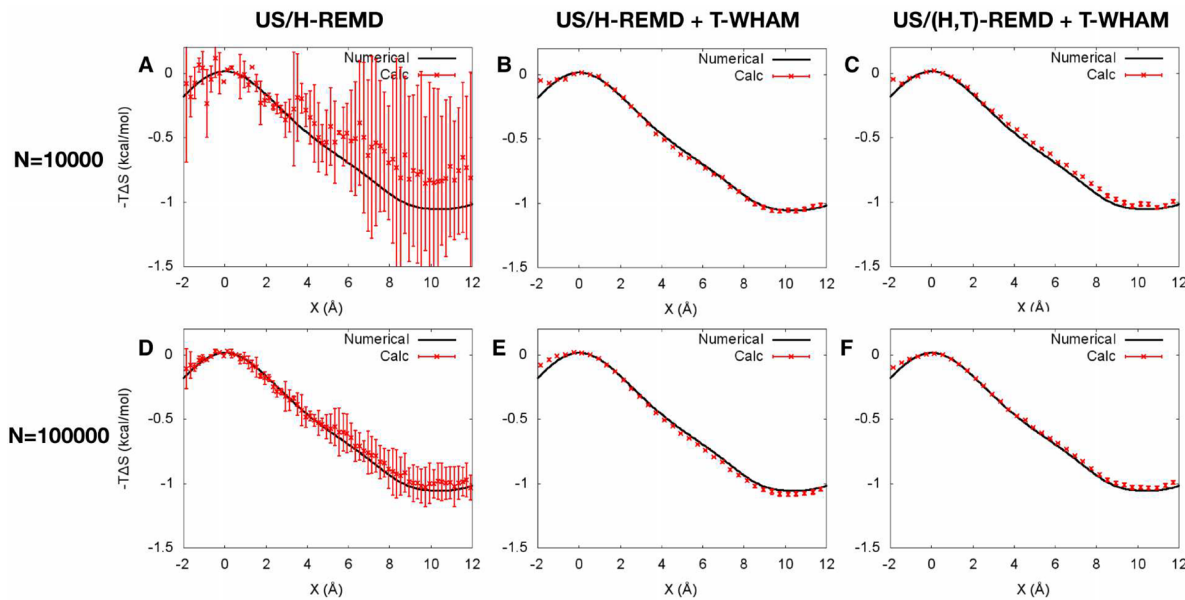


Figure 2. Entropy profile ($T = 346.41\text{ K}$) of the toy simulation system derived with different numbers of data points, $N = 10\,000$ (top) and $N = 100\,000$ (bottom), starting from the beginning of the simulations. Entropy estimated from independent simulations and analyzed with (A, D) conventional WHAM and (B, E) T-WHAM. (C, F) Entropy estimated from REMD simulations and analyzed with T-WHAM.

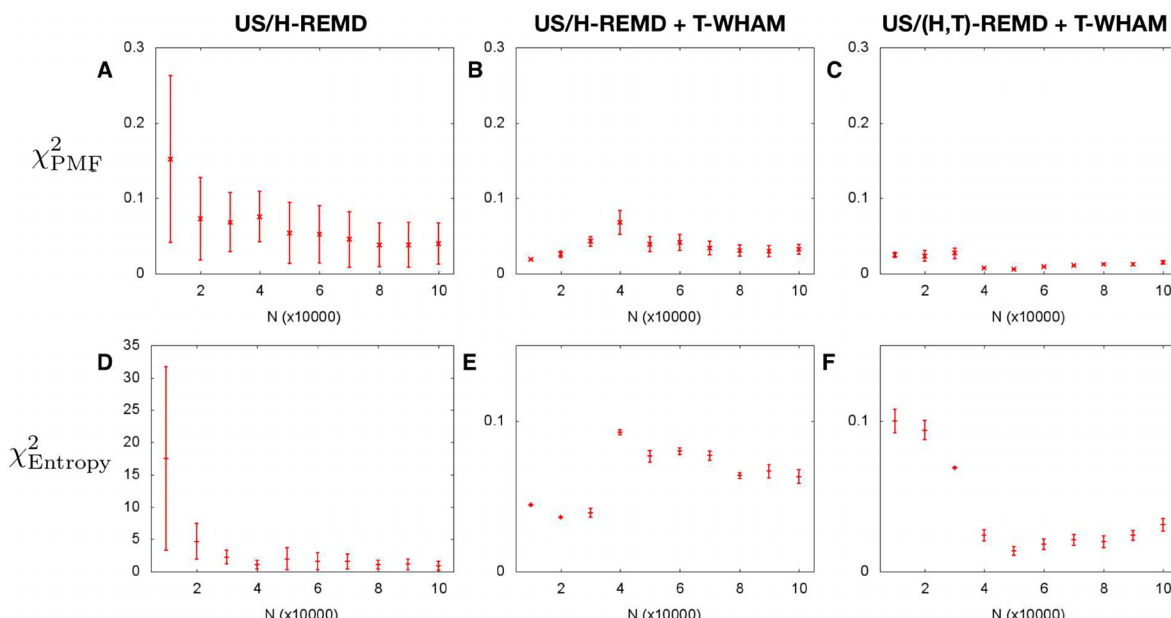


Figure 3. Absolute errors in the PMFs (A–C) and entropy (D–F) obtained from the MD simulations. The absolute errors are calculated as $\chi^2 = \sum_{\eta} (O(\eta) - E(\eta))^2$, where O and E represent observed and expected values, respectively, e.g., PMF and entropy. Hence, the unit of the absolute error is $(\text{kcal/mol})^2$. The absolute errors were measured with an increasing number of data points, N , starting from the beginning of the simulations. The error bars are the standard deviation of χ^2 from individual error estimates.

In multiple-walker ABF simulations, the model reaction coordinate was explored over a single window ranging from $r = 3$ to 12 \AA , discretized in small bins, 0.1 \AA wide, in which samples of the instantaneous force were accrued. No biasing force was applied before a minimum of 1000 samples were collected in a given bin. Reversible association of the two methane molecules was examined at five temperatures, 288, 293, 298, 303, and 308 K . For each temperature, 10 replicas were used, which exchanged information every 1000 molecular dynamics steps.

RESULTS AND DISCUSSION

Illustration Efficient Entropy Determination Using a Simplified Model. Using the toy model, US MD simulations were performed at three different temperatures (300, 346.41, and 400 K), and the resulting 1D PMFs along the x coordinates were used to estimate the entropy using the FD approach. Three different schemes were employed to assess their relative efficiency in entropy estimation: (i) three independent US/ \mathcal{H} -REMD simulations analyzed with WHAM, (ii) three independent US/ \mathcal{H} -REMD simulations analyzed with T-WHAM, and (iii) US/(\mathcal{H}, T)-REMD using three temperatures

analyzed with T-WHAM. The time interval of attempted exchange was set to 20 steps, and the position of the particles was recorded at the same frequency for the postanalysis.

For all three methods, the PMFs derived from the MD simulations match the numerically derived PMFs well (see below for further discussion). However, the estimated entropy from US/ \mathcal{H} -REMD and WHAM was considerably worse than the other two methods. Figure 2 shows the entropy estimated at different numbers of data points, namely, 10 000 and 100 000, starting from the beginning of the simulations. The estimated entropies from US/ \mathcal{H} -REMD + T-WHAM and US/ (\mathcal{H},T) -REMD + T-WHAM match well with the numerically estimated entropy, even when there are only 10 000 data points. On the other hand, the estimated entropy from US/ \mathcal{H} -REMD + WHAM appears to be quite noisy and slowly converging, even after 100 000 data points.

To better understand how different approaches enhance ergodic sampling, we have calculated the absolute errors associated in the PMFs and entropies using a straightforward χ^2 test. Figure 3 shows the changes of χ^2 with respect to the number of data points used in the analysis. Again, for all three methods, the PMFs match the numerically derived PMFs well, even for a number of data points as low as $N = 10\,000$, although the error bars from the US/ \mathcal{H} -REMD + WHAM are fairly large compared to those from the other two methods. However, these small errors in the PMFs are amplified upon entropy estimation via FD, and χ^2_{entropy} of US/ \mathcal{H} -REMD + WHAM clearly shows large error in the estimated entropy.

The improvement of US/ (\mathcal{H},T) -REMD + T-WHAM and US/ \mathcal{H} -REMD + T-WHAM relative to US/ \mathcal{H} -REMD + WHAM raises the question as to what could be the source of enhancement. Figure 4 shows the ratio of χ^2_{PMF} observed from US/ \mathcal{H} -REMD + T-WHAM and US/ (\mathcal{H},T) -REMD + T-WHAM relative to the ones observed from US/ \mathcal{H} -REMD + WHAM. The error ratio smaller than one indicates that the comparing method has improved χ^2 values smaller than the ones from US/ \mathcal{H} -REMD + WHAM. It appears that the application of T-WHAM can reduce the error in both PMF and entropy estimations only by about an order of magnitude. T-WHAM combines the data produced by multiple simulations carried out at different temperatures; therefore, it enhances the performance of the entropy estimation. In our simulation, we have combined three temperatures, and the error ratio suggests that US/ \mathcal{H} -REMD + WHAM needs at least 3 to 4 times more data points to have a similar level of error in PMF compared to that with US/ \mathcal{H} -REMD + T-WHAM, which is not unexpected. In addition, T-REMD can be effective in sampling rare configurations and overcoming energetic barriers. In our toy model, T-REMD appears to further reduce the error by about 2- to 3-fold. Improvements of χ^2_{entropy} are much greater (more than 10-fold) when T-WHAM or T-REMD were used. This result is in line with the previous findings by Rick,¹⁴ where application of T-WHAM significantly enhanced the performance for both PMFs and entropy estimations.

Performance of PINS in Entropy Estimation. The performance of PINS and several of its variants was tested in terms of absolute error in the calculated PMF/entropy as well as their execution times. Table 1 shows the complete list of test simulations that we have performed: (i) PINS with block sizes of 6 and 4, (ii) M-PINS with a block size of 4, and (iii) hybrid-PINS where regular neighbor-exchange REMD is performed along the umbrella bias windows and M-PINS is performed

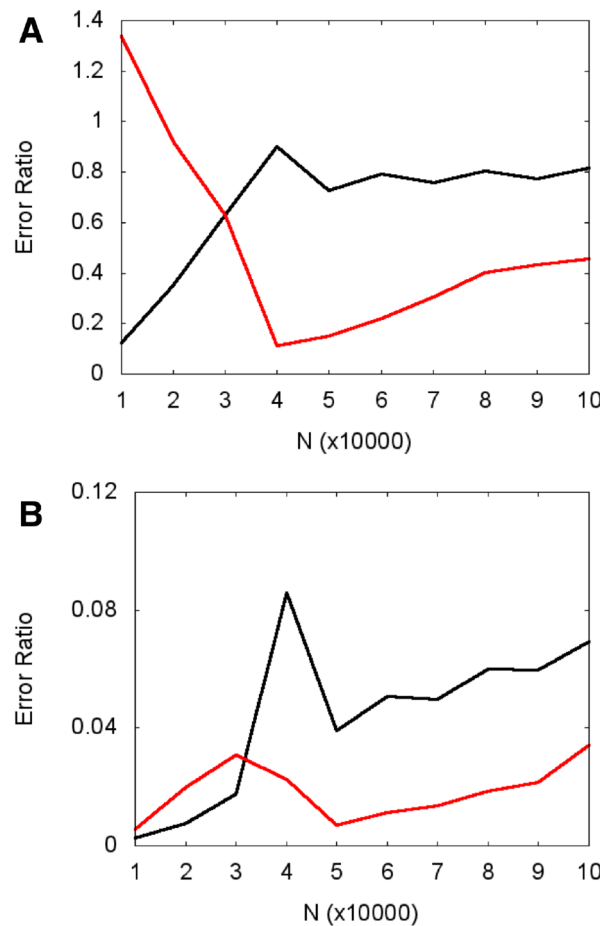


Figure 4. Ratio of χ^2_{PMF} (A) and χ^2_{entropy} (B) observed from US/ \mathcal{H} -REMD + T-WHAM (black curve) and US/ (\mathcal{H},T) -REMD + T-WHAM (red curve) relative to the χ^2 observed from US/ \mathcal{H} -REMD + WHAM.

Table 1. Test Cases for PINS and Variants of PINS^a

	block size	execution time (s)
US/ (\mathcal{H},T) -REMD	2	1202
PINS	6 (2/3)	28 838
	4 (2/2)	2367
M-PINS	4 (2/2)	2486
hybrid INS/REMD	2/3	2018

^aBlock size is the number of replicas in each block, and the number in the parentheses represents the number of replicas in the bias and temperature dimensions.

along the temperature windows in alternating cycles. Figure 5 shows both the absolute error of various PINS methods and the error ratio relative to the US/ (\mathcal{H},T) -REMD method. Although different variants gave slightly different results, in general, PINS and its variants performed on par with or slightly better than US/ (\mathcal{H},T) -REMD in terms of absolute errors in PMFs and entropy. In particular, the PINS with 6 replicas in a block and hybrid-PINS methods performed well, which can be also confirmed in the χ^2 error ratio relative to the χ^2 from US/ (\mathcal{H},T) -REMD simulations (see green curve in Figure 5B,D). Reducing the number of replicas in a block increases the error in the PMFs and entropy initially. However, as the data points accumulate, the algorithm approaches a similar level of accuracy as that of the other methods. M-PINS performs well

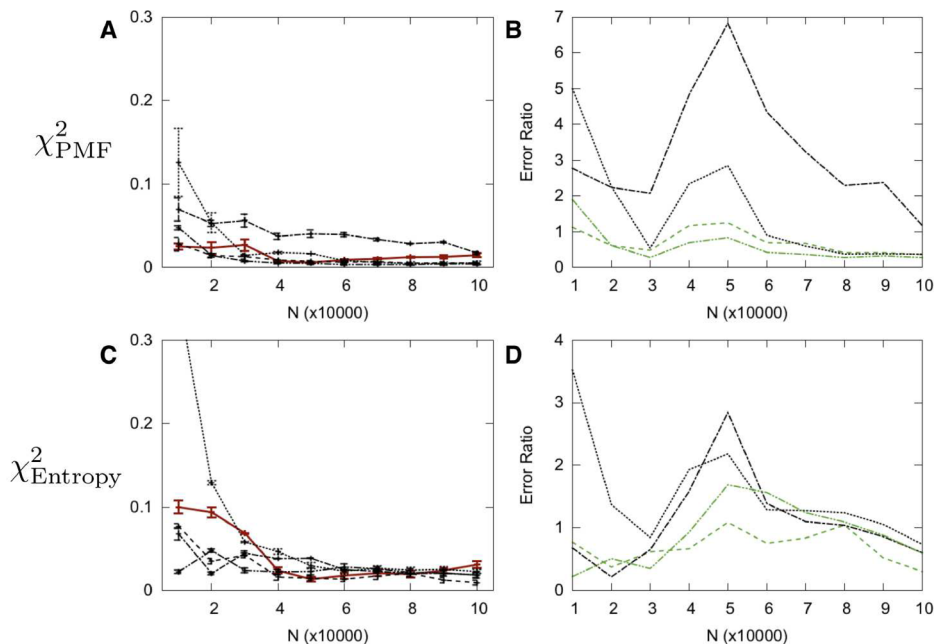


Figure 5. Absolute errors in (A) PMFs and (C) entropy obtained from various PINS and its variants compared to US/(H, T)-REMD + T-WHAM (solid red line): PINS with block size of 6 (dashed) and 4 (dotted line), M-PINS (dashed-dot line), and hybrid-PINS (dashed-dot-dot line). (B, D) χ^2 ratio of various PINS and its variants relative the one from US/(H, T)-REMD + T-WHAM simulation. The results from PINS with a block size of 6 and hybrid-PINS are highlighted using a green color.

in entropy estimation, but it showed slightly elevated levels of error associated with the PMFs. It should be noted that the absolute errors are all very small and the analysis is based on a single performance test; attention, therefore, must be paid when comparing the results inferred from different PINS schemes.

PINS and its variants exhibit longer execution times because of the greater amount of communication within the replica in the same block and the increased number of energy evaluations for different umbrella windows. In addition, the permutation probability for all possible arrangements of replica conditions has to be evaluated. As a result, PINS with 6 replicas in a block, which requires $6! = 720$ permutation probability calculation, takes more than 20 times longer than conventional neighbor exchange REMD. If we restrain the block size to 4, then the execution time is only about twice as long as that of regular REMD. Considering that our toy model is rudimentary, the overhead can diminish in real biological systems, where integrating the equation of motion takes a considerable amount of time.

Methane Binding Entropy. Small hydrophobic molecules, such as methane, possess a favorable free energy for dimer formation in polar solvents.¹ Simulations and theoretical models have explained that the favorable entropic contribution of solvent molecules is the dominant driving force behind the association of such small hydrophobic species.^{2,49–53} The hydrophobic interaction of nonpolar molecules has a significant implication on protein folding and aggregation of misfolded proteins.⁵⁴ Therefore, an accurate description of the association in terms of thermodynamic components, e.g., enthalpy and entropy, is of paramount importance. Several simulations have already tried to tackle this problem using MD simulations,^{2,49,50,52} but the accuracy of the entropy calculation has remained the main stumbling block. We have applied the US/(H, T)-REMD method, which can considerably reduce the

error in the estimated entropy, to the methane binding free energy and entropy calculation. In addition, we have compared our results with those inferred from multiple-walker ABF simulations and discussed the accuracy of the entropy obtained with an alternate method.

We have used explicit methane molecules and performed 60 ns of US/(H, T)-REMD simulation in an explicit water box with five different temperatures ranging from 295 to 305 K. Figure 6 shows well-converged PMFs and the entropy along the intermolecular distance of two methane molecules' reaction coordinates. We have found two PMF minima around intermolecular distances of 3.9 Å (contact minimum) and 7.3 Å (solvent-separated minimum). The contact minimum and the solvent-separated minimum have well depths of -0.75 and -0.08 kcal/mol at 300 K, respectively, and are separated by a barrier about 1 kcal/mol high. These features in the PMF match quite well those in the PMFs obtained from various earlier simulations and theoretical studies, notwithstanding the fact that methane-like pseudoatoms were utilized in these earlier investigations.^{2,49–53}

By running the simulations at different temperatures, we observed the effect of the entropic contribution on the free energy profile. As shown in Figure 6, the well depth of the PMF increases and the barrier height decreases as the temperature of the system increases, suggesting a favorable entropic contribution. Similar to the PMF, the entropy profile possesses two minima: one coincides with the contact minimum but is much wider and the other is found around 8.5 Å, where free energy is slightly unfavorable. This behavior could be linked to the thermodynamics of solvation of small hydrophobic molecules. It is well-known that solvation of small hydrophobic species induces ordering of solvent molecules around it, which is entropically unfavorable.^{43,54–56} Bringing two isolated solutes results in expelled solvent molecules, which increases the volume of the system and the overall entropy of the system.

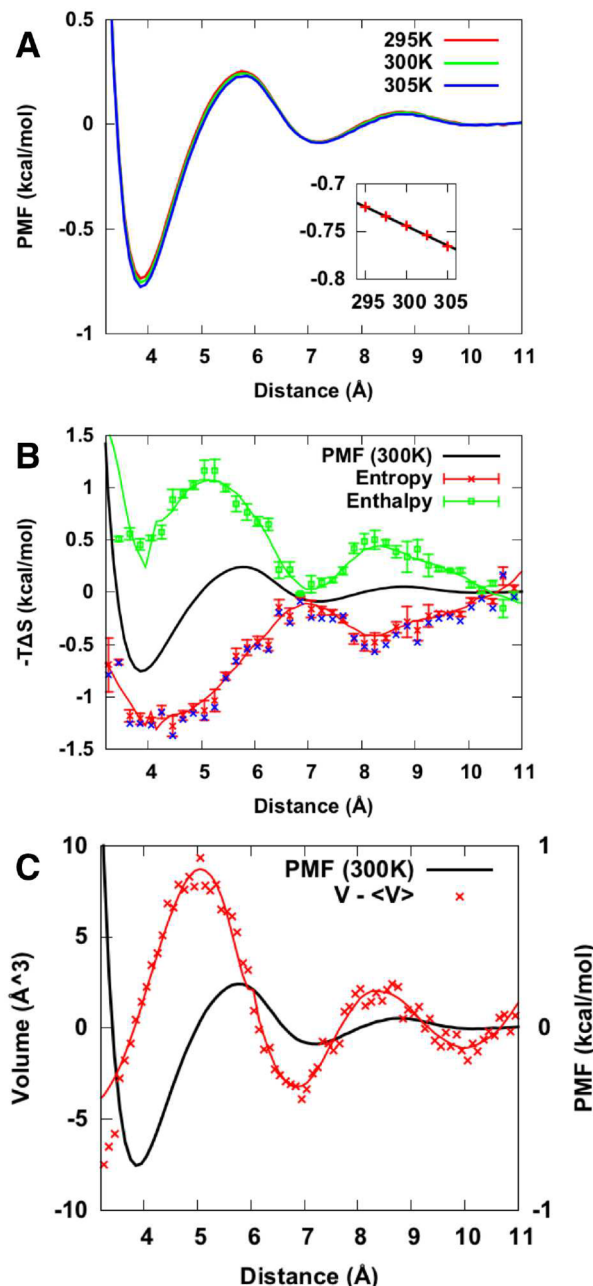


Figure 6. PMF (A) and entropy (B) of methane association in TIP3P water. The error bars in entropy are the standard deviation of entropies estimated by different pairs of PMFs. Blue crosses are the entropy estimation using eq 6. The inset in (A) shows the temperature dependence of PMF at $r = 3.95 \text{ \AA}$. The solid line is obtained by the linear regression of the PMF values at different temperatures. (C) Volume change along the reaction coordinate. $\langle V \rangle$ is calculated by taking the average of the volumes when the two solutes are fully separated ($r = 11.0 \text{ \AA}$). The solid curves are obtained by applying a Savitzky–Golay smoothing filter.

While the expulsion of the solvent around the hydrophobic solute is entropically favorable, it is enthalpically unfavorable due to disruption of the hydrogen-bonding network of solvent molecules. The reported value of the height of the entropic barrier relative to the minimum varies in the literature (1.0–2.5 kcal/mol).^{2,49–53} Our US/(\mathcal{H}, T)-REMD showed an entropic barrier height of about 1.3 kcal/mol relative to the minimum,

and the entropic contribution still remains slightly favorable at the barrier.

We have performed the simulation in an isobaric ensemble, and, thus, we could further decompose the entropic contribution to energetic and, so-called, pV work contributions, i.e., $-T\Delta S = \Delta G - \Delta H = \Delta G - \Delta U - p\Delta V$. We have performed a T -WHAM analysis with an explicit pV term, and the WHAM-weighted average volume and energy along the reaction coordinates were calculated. Interestingly, the volume of the simulation system is affected by the reaction coordinate. As we examine the volume change along the reaction coordinates, $V(r) - \langle V(r = \infty) \rangle$, the volume increases as the methane molecules are moving apart and maximizes near the barrier separating the contact and the solvent-separated minima, which implies an increasing empty volume between the two solutes. The volume of the system decreases as the two methane molecules are stabilized at the solvent-separated minimum, suggestive of a tight packing of water around the methane molecules. Still, the volume change is too small to contribute in a meaningful sense to the total free energy, <1.5 cal/mol when 10 \AA^3 of the volume changes at atmospheric pressure. However, it would be interesting to compare the pV work component in larger systems, e.g., protein–protein binding, where the volume change is expected to be appreciably larger.

Typically, simulation trajectories are divided, and sub-blocks of trajectories are used to probe convergence. We have divided the US/(\mathcal{H}, T)-REMD trajectories and compared the entropy profiles obtained with different lengths of sub-blocks. To easily compare the differences in free energy and entropy profiles using different sub-block sizes, we have calculated the association free energy using $\Delta G(\beta) = \int_{r_0=1.5}^{r_0+1.5} \exp[-\beta \Delta W(r)]$, where $\Delta W(r) = W(r) - W(r = \infty)$ and r_0 is the separation at the free energy minimum. The association entropy was calculated from FD of association free energies. As shown in Figure 7, the association free energy converges quickly within the first nanosecond of simulation, and the quantities remain consistent regardless of the sub-block size used. However, the entropy converges much slower, and at least a 10 ns block size is required to obtain consistent association entropy values with less than 0.5 kcal/mol fluctuation.

Quantitative measurement of the association free energy of a methane molecule is extremely challenging. Yaacobi and Ben-Naim measured the thermodynamics of methane and ethane in water and inferred the free energy and entropy of methane dimer formation to be 2.17 and 3.3 kcal/mol, respectively, at 298 K.¹ Their estimation is based on the assumption that the CH_3- group in an ethane molecule will interact with the surrounding solvent in the same manner as that of a methane molecule. Although ethane and methane dimers exhibit similar physicochemical properties, the measurements under this assumption produce thermodynamics, association free energy and entropy, at bond distance around 1.54 Å, which is more than 2 Å shorter than the contact minimum observed in a methane dimer.

We have also performed a set of independent simulations based on the multiple-walker ABF algorithm^{38,39} at different temperatures. The method runs several simulations concomitantly and combines the adaptive forces from each simulation to explore the free energy surface along the reaction coordinate faster. The ABF algorithm has already demonstrated that it can quickly produce reliable free energy profiles,¹⁵ thus, it would be

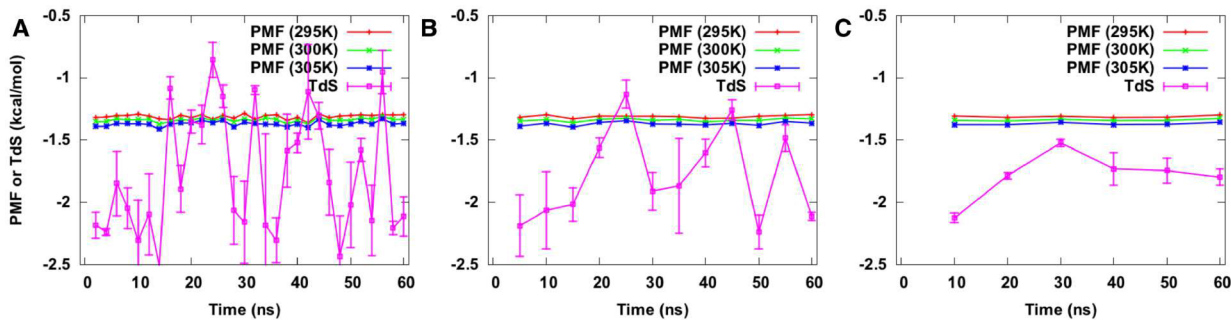


Figure 7. Association free energy and entropy using different nonoverlapping sub-block sizes of the trajectory employed: (A) 2, (B) 5, and (C) 10 ns. The error bar associated with the entropy is the standard deviation calculated by choosing all possible pairs of free energies at different temperatures.

instructive to compare the accuracy of entropy estimations based on independent trajectories at different temperature. Figure 8 shows the PMFs and estimated entropy. The PMFs

error associated with the entropy profile obtained from independent simulations is large and reaches a magnitude of nearly 1 kcal/mol.

Upon inspection, the primary source of this large error appears to be the slight variations in the PMFs caused by statistical inaccuracies. Entropies are calculated by $T\Delta S = T(\Delta G(T + \Delta T) - \Delta G(T - \Delta T))/(2\Delta T)$, and small fluctuations in ΔG , as little as 0.05 kcal/mol, are amplified to as much as 1.06 kcal/mol in $T\Delta S$ when $\Delta T = 10$ and 300 K are used. To avoid large statistical uncertainty, larger temperature gaps can, in principle, be used. In fact, the entropy profile calculated from the simulations performed at the highest and the lowest temperatures showed only a small deviation (<0.1 kcal/mol), especially after 40 ns of simulation time (see Figure S1). Methods that enhance the internal consistency of the statistical ensemble increase the efficiency of entropy estimation and allow simulations to be performed with a smaller temperature increment. It should be noted that these methods, such as *T*-WHAM and replica-exchange, increase correlation between PMFs and that the statistical uncertainty could be underestimated depending on the error analysis method (see Figure S2).

Finally, the performance of different replica-exchange algorithms was tested. A two-dimensional PINS simulation with a block size of 6 (2 umbrellas \times 3 temperatures) and a hybrid-INS simulation (neighbor exchange along umbrellas and INS for temperature windows) were performed using 30 ns simulations and the same number of replicas as that with *T*-REMD. Both PINS and hybrid-INS increased the total execution time around 4-fold compared to that of *T*-REMD simulations due to the increased amount of communication and energy evaluation. Figures S3 shows the comparison of the association free energy calculated from *T*-REMD, PINS, and hybrid-INS algorithms. The convergence of PMFs and entropy obtained from the PINS and hybrid-INS methods remained at a level similar to that of *T*-REMD.

CONCLUSIONS

Free energy methodologies have been greatly improved in the past decade and are now widely used in many physical sciences research areas. However, an accurate determination of entropy still represents a daunting, computationally challenging task. Here, we have quantitatively tested the performance of different computational approaches to estimate entropy using a simple toy model. The performance of these approaches applied to entropy estimation, in terms of accuracy and convergence, can be greatly improved in two ways: first, by combining the

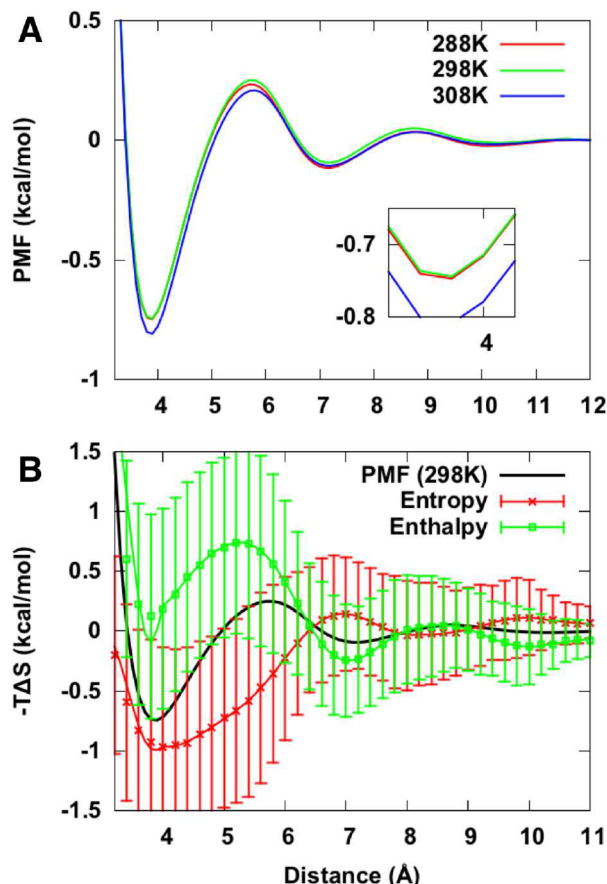


Figure 8. (A) PMF and (B) entropy of methane association in TIP3P water using multiple-walker ABF algorithms. The error bars in entropy are the standard deviation of entropies estimated by different pairs of PMFs. The solid curves are obtained by applying a Savitzky–Golay smoothing filter.

determined from the US/(H, T)-REMD or ABF algorithm show similar features, specifically two minima around intermolecular distances of 3.9 and 7.3 Å separated by a barrier about 1 kcal/mol high. The average entropy profile from both methods also reveals similar features, namely, a favorable entropic contribution at the contact minimum and an entropic barrier at the solvent-separated minimum. Yet, the estimated

simulations carried out at different temperatures using *T*-WHAM. Without any additional simulations, the accuracy and convergence of both PMFs and entropy are improved dramatically. Second, the performance is improved by coupling the simulations running at different temperatures using *T*-REMD. Doing so requires some planning and computational resources, but increased accuracy can be expected owing to the enhanced sampling of phase space, particularly for complex biomolecular systems.

We have also tested the performance of the INS method and several of its variants. INS allows the swapping of replicas that are not necessarily nearest neighbors as well as a faster rate of travel for replicas in the multiple copy space. However, for biomolecular systems composed of a large number of umbrella sampling windows, INS cannot be applied in a straightforward fashion. To address this limitation, the PINS method is proposed, which divides the replica windows into non-overlapping blocks so that INS is performed only within a given block. In our tests, the PINS method with large block sizes performed slightly better than regular neighbor-exchange REMD methods. However, the overhead from computing permutation probability could be prohibitively expensive. Among the other variants tested herein, the hybrid-INS/REMD method, in which REMD is performed along the umbrella bias windows and M-PINS is performed along the temperature windows in an alternating fashion, also performed well.

Finally, we have carried out simulations of the reversible association of two methane molecules in liquid water and decomposed the free energy profile into entropic and enthalpic contributions. Adopting *T*-REMD for efficient sampling and *T*-WHAM for analysis yielded consistent, accurate entropy profiles along the intermolecular distance between two methane molecules. Within the first nanosecond, the PMF appears to be well-converged. In contrast, the entropy converges much more slowly, requiring significantly more data points, about 10 times more, to provide a reliable estimate. More advanced replica-exchange algorithms, such as PINS and hybrid-INS/REMD, were applied to the same simulation setup; however, no significant enhancement were observed in the final entropy estimation.

Independent simulations carried out at different temperatures appear to generate larger statistical errors associated with the estimation of entropy. The simulations performed with a multiple-walker version of the ABF algorithm tend to suggest that, while multiple-replica strategies effectively enhance ergodic sampling by populating marginally visited regions of the free energy landscape, exchange of configurations characterized by different temperatures appears to be equally crucial. They also illustrate the dilemma of the practitioner in choosing an appropriate temperature increment for entropy estimations based on finite differences of the free energy; exaggeratedly small increments yield free energy differences on the order of associated statistical error, whereas too large increments are incompatible with the assumption that underlies FD. *T*-WHAM and replica-exchange schemes were shown to produce more consistent free energy profiles for different temperatures and yield smaller statistical errors in estimated entropies even though smaller temperature gaps were used.

ASSOCIATED CONTENT

S Supporting Information

RMSD error of the entropy profile obtained from multiple walker ABF simulations (Figure S1), comparison of alternate replica-exchange algorithms (Figure S2), and association free energy and entropy using different nonoverlapping sub-block sizes of the trajectory employed (Figure S3). This material is available free of charge via the Internet at <http://pubs.acs.org>.

AUTHOR INFORMATION

Corresponding Author

*E-mail: roux@uchicago.edu

Notes

The authors declare no competing financial interest.

ACKNOWLEDGMENTS

This research used resources of the Argonne Leadership Computing Facility, which is a DOE Office of Science User Facility supported under contract DE-AC02-06CH11357. We gratefully acknowledge the computing resources provided on Fusion, a high-performance computing cluster operated by the Laboratory Computing Resource Center at Argonne National Laboratory. The Centre Informatique National de l'Enseignement Supérieur, Montpellier, is also gratefully acknowledged for the generous provision of computer time. The authors are indebted to the France and Chicago Collaborating in the Sciences (FACCTS) Center for their support.

REFERENCES

- (1) Yaacobi, M.; Ben-Naim, A. *J. Phys. Chem.* **1974**, *78*, 175–178.
- (2) Smith, D. E.; Zhang, L.; Haymet, A. D. J. *J. Am. Chem. Soc.* **1992**, *114*, 8875–8876.
- (3) Chang, C.-E. A.; McLaughlin, W. A.; Baron, R.; Wang, W.; McCammon, J. A. *Proc. Natl. Acad. Sci. U.S.A.* **2008**, *105*, 7456–7461.
- (4) Monod, J.; Wyman, J.; Changeux, J.-P. *J. Mol. Biol.* **1965**, *12*, 88–118.
- (5) Cooper, A.; Dryden, D. T. F. *Eur. Biophys. J.* **1984**, *11*, 103–109.
- (6) Frederick, K. K.; Marlow, M. S.; Valentine, K. G.; Wand, A. J. *Nature* **2007**, *448*, 325–329.
- (7) Freire, E. *Drug Discovery Today* **2008**, *13*, 869–874.
- (8) DeLorbe, J. E.; Clements, J. H.; Teresk, M. G.; Benfield, A. P.; Plake, H. R.; Millspaugh, L. E.; Martin, S. F. *J. Am. Chem. Soc.* **2009**, *131*, 16758–16770.
- (9) Pearlman, D. A.; Rao, B. G. *Encyclopedia of Computational Chemistry*; John Wiley & Sons, Ltd: Chichester, UK, 2002; pp 1036–1058.
- (10) Lu, N.; Kofke, D. A.; Woolf, T. B. *J. Phys. Chem. B* **2003**, *107*, 5598–5611.
- (11) Smith, D. E.; Haymet, A. D. J. *J. Chem. Phys.* **1993**, *98*, 6445–6454.
- (12) MacCallum, J. L.; Tielemans, D. P. *J. Am. Chem. Soc.* **2006**, *128*, 125–130.
- (13) Baron, R.; Setny, P.; McCammon, J. A. *J. Am. Chem. Soc.* **2010**, *132*, 12091–12097.
- (14) Rick, S. W. *J. Chem. Theory Comput.* **2006**, *2*, 939–946.
- (15) Comer, J.; Roux, B.; Chipot, C. *Mol. Simul.* **2014**, *40*, 218–228.
- (16) Makhatadze, G. I.; Privalov, P. L. *J. Chem. Thermodyn.* **1988**, *20*, 405–412.
- (17) Sugita, Y.; Okamoto, Y. *Chem. Phys. Lett.* **1999**, *314*, 141–151.
- (18) Gallicchio, E.; Andrec, M.; Felts, A. K.; Levy, R. M. *J. Phys. Chem. B* **2005**, *109*, 6722–6731.
- (19) Chodera, J. D.; Swope, W. C.; Pitera, J. W.; Seok, C.; Dill, K. A. *J. Chem. Theory Comput.* **2007**, *3*, 26–41.
- (20) Laghaei, R.; Mousseau, N.; Wei, G. *J. Phys. Chem. B* **2010**, *114*, 7071–7077.

- (21) Laghaei, R.; Mousseau, N.; Wei, G. *J. Phys. Chem. B* **2011**, *115*, 3146–3154.
- (22) Ferrenberg, A.; Swendsen, R. *Phys. Rev. Lett.* **1989**, *63*, 1195–1198.
- (23) Kumar, S.; Bouzida, D.; Swendsen, R.; Kollman, P. A.; Rosenberg, J. *J. Comput. Chem.* **1992**, *13*, 1011–1021.
- (24) Souaille, M.; Roux, B. *Comput. Phys. Commun.* **2001**, *135*, 40–57.
- (25) Sindhikara, D.; Meng, Y.; Roitberg, A. E. *J. Chem. Phys.* **2008**, *128*, 024103.
- (26) Abraham, M. J.; Gready, J. E. *J. Chem. Theory Comput.* **2008**, *4*, 1119–1128.
- (27) Dupuis, P.; Liu, Y.; Plattner, N.; Doll, J. D. *Multiscale Model. Simul.* **2012**, *10*, 986–1022.
- (28) Plattner, N.; Doll, J. D.; Meuwly, M. *J. Chem. Theory Comput.* **2013**, *9*, 4215–4224.
- (29) Plattner, N.; Doll, J. D.; Dupuis, P.; Wang, H.; Liu, Y.; Gubernatis, J. E. *J. Chem. Phys.* **2011**, *135*, 134111.
- (30) Chodera, J. D.; Shirts, M. R. *J. Chem. Phys.* **2011**, *135*, 194110.
- (31) Rodinger, T.; Howell, P. L.; Pomès, R. *J. Chem. Theory Comput.* **2006**, *2*, 725–731.
- (32) Rosta, E.; Hummer, G. *J. Chem. Phys.* **2010**, *132*, 034102.
- (33) Liu, J. S. *Biometrika* **1996**, *83*, 681–682.
- (34) Darve, E.; Pohorille, A. *J. Chem. Phys.* **2001**, *115*, 9169.
- (35) Hénin, J.; Chipot, C. *J. Chem. Phys.* **2004**, *121*, 2904–2914.
- (36) Chipot, C. *Wiley Interdiscip. Rev.: Comput. Mol. Sci.* **2014**, *4*, 71–89.
- (37) Zheng, L.; Chen, M.; Yang, W. *Proc. Natl. Acad. Sci. U.S.A.* **2008**, *105*, 20227–20232.
- (38) Minoukadeh, K.; Chipot, C.; Lelièvre, T. *J. Chem. Theory Comput.* **2010**, *6*, 1008–1017.
- (39) Comer, J.; Phillips, J. C.; Schulten, K.; Chipot, C. *J. Chem. Theory Comput.* **2014**, *10*, 5276–5285.
- (40) Phillips, J. C.; Braun, R.; Wang, W.; Gumbart, J. C.; Tajkhorshid, E.; Villa, E.; Chipot, C.; Skeel, R. D.; Kalé, L.; Schulten, K. *J. Comput. Chem.* **2005**, *26*, 1781–1802.
- (41) Vanommeslaeghe, K.; Hatcher, E. R.; Acharya, C.; Kundu, S.; Zhong, S.; Shim, J.; Darian, E.; Guvench, O.; Lopes, P.; Vorobyov, I.; MacKerell, A. D., Jr. *J. Comput. Chem.* **2010**, *31*, 671–690.
- (42) Jorgensen, W. L.; Chandrasekhar, J.; Madura, J. D.; Impey, R. W.; Klein, M. L. *J. Chem. Phys.* **1983**, *79*, 926.
- (43) Durell, S. R.; Brooks, B. R.; Ben-Naim, A. *J. Phys. Chem.* **1994**, *98*, 2198–2202.
- (44) Ryckaert, J.-P.; Ciccotti, G.; Berendsen, H. J. C. *J. Comput. Phys.* **1977**, *23*, 327–341.
- (45) Steinbach, P. J.; Brooks, B. R. *J. Comput. Chem.* **1994**, *15*, 667–683.
- (46) Essmann, U.; Perera, L.; Berkowitz, M. L.; Darden, T.; Lee, H.; Pedersen, L. G. *J. Chem. Phys.* **1995**, *103*, 8577–8593.
- (47) Feller, S. E.; Zhang, Y.; Pastor, R. W.; Brooks, B. R. *J. Chem. Phys.* **1995**, *103*, 4613.
- (48) Martyna, G. J.; Tobias, D. J.; Klein, M. L. *J. Chem. Phys.* **1994**, *101*, 4177.
- (49) Ludemann, S.; Schreiber, H.; Abseher, R.; Steinhauser, O. *J. Chem. Phys.* **1996**, *104*, 286.
- (50) Garde, S.; Hummer, G.; Paulaitis, M. E. *Faraday Disc.* **1996**, *103*, 125.
- (51) Hummer, G.; Garde, S.; García, A. E.; Pohorille, A.; Pratt, L. R. *Proc. Natl. Acad. Sci. U.S.A.* **1996**, *93*, 8951–8955.
- (52) Ghosh, T.; García, A. E.; Garde, S. *J. Chem. Phys.* **2002**, *116*, 2480–2486.
- (53) Morozov, A. N.; Lin, S. H. *J. Chem. Phys.* **2009**, *130*, 074903.
- (54) Chandler, D. *Nature* **2005**, *437*, 640–647.
- (55) Pratt, L. R.; Chandler, D. *J. Chem. Phys.* **1977**, *67*, 3683.
- (56) Galamba, N. *J. Phys. Chem. B* **2013**, *117*, 2153–2159.